Rapid #: -19423074

CROSS REF ID: **975045**

LENDER: **U@M :: Main Library**

BORROWER: **EYW :: Main Library**

TYPE:	Article CC:CCG
JOURNAL TITLE:	Combustion and flame
USER JOURNAL TITLE:	Combustion and Flame
ARTICLE TITLE:	Initiation and propagation of one-dimensional planar flames in mixtures with variable reaction progress
ARTICLE AUTHOR:	Xiao, Gan
VOLUME:	236
ISSUE:	
MONTH:	
YEAR:	2022
PAGES:	111765-
ISSN:	0010-2180
OCLC #:	

Processed by RapidX: 8/22/2022 4:06:15 AM

Combustion and Flame 236 (2022) 111765

Contents lists available at ScienceDirect

Combustion and Flame

journal homepage: www.elsevier.com/locate/combustflame

Initiation and propagation of one-dimensional planar flames in mixtures with variable reaction progress

Gan Xiao[a], Haiwen Ge[b], Peng Zhao[a,*]

[a] Department of Mechanical, Aerospace & Biomedical Engineering, UT Space Institute, University of Tennessee, Knoxville, TN 37388 USA
[b] Department of Mechanical Engineering, Texas Tech University, Lubbock, TX, USA

ARTICLE INFO

Article history:
Received 16 May 2021
Revised 17 September 2021
Accepted 18 September 2021
Available online 3 October 2021

Keywords:
Ignition energy
Ignition timing
Flame initiation
Cool flame
Autoignition-assisted flame
Low temperature chemistry

ABSTRACT

In light of the recent high temperature flame experiment conducted in a shock tube, the main objective of the present study is to understand flame initiation regimes and propagation features with various ignition energy and various extents of unburnt mixture reaction progress. Flame initiation and propagation are numerically investigated for a partially reactive, near stoichiometric n-heptane/air/He mixtures under elevated temperature 700 K in a one-dimensional planar domain under nearly isobaric condition. Emphasis on flame initiation is placed on the effects of ignition energy and initial reaction progress. For ignition timing at $t_{ig} = 0$ s, while regular hot flames are directly initiated with higher ignition energy as expected, a class of autoignition-assisted cool flames can be directly triggered with relatively low ignition energy. By postponing ignition at later times, more pronounced chemical reaction progress is associated with the unburnt mixture such that autoignition-assisted hot flame can be achieved. For such flames, a notable flame speed increment is observed after the first-stage ignition occurs in the upstream unburnt mixture. It is found that both autoignition-assisted cool and hot flames prior to the first-stage ignition strongly depend on the ignition energy and ignition timing, and hence are case-sensitive. Extra caution needs to be taken to evaluate and compare these data. Hot flames in the post first-stage ignition mixture nevertheless exhibit much less variation to the ignition energy and initial reaction progress. For steady-state simulation, it is emphasized that a sufficiently short upstream and sufficiently long downstream domain are needed to obtain desired flame solution in the classical diffusion-reaction limit. A good agreement between the steady and unsteady simulations demonstrates the unsteady flame propagates in a quasi-steady manner with the classical flame structure, *as long as* $\tau_{chem}/\tau_{flame} >> 1$. Sensitivity analysis and reaction network analysis have further suggested the similar key reactions on flame speed compared with regular conditions and demonstrated indirect effects from the low temperature ignition chemistry. This work provides useful insights into flame initiation regimes and propagation features under elevated temperature.

1. Introduction

Initiation and propagation characteristics of laminar flames are key thermal-chemical properties of a reacting mixture and have been main themes of combustion research [1–5]. As combustion research becomes increasingly quantitative, laboratory burners with various well-defined flame configurations including flat flame [6], Bunsen flame [7], counterflow flame [8], spherical flame [9] have been developed to measure the flame speed with the assistance of laser diagnostic tools. However, most of the experimental data acquired are unfortunately limited to chemically frozen mixtures under room or only slightly elevated temperatures, which are substantially lower compared to flame conditions under conventional practical combustors in internal combustion engines, gas turbines, ram- and scram- jet engines. Due to the elevated ambient temperature, the unburnt mixture in practical systems is partially reactive and can lead to substantial gaps to the understanding of practical flame behaviors, the development of advanced combustion strategies like spark assisted compression ignition (SACI) [10], as well as prediction of abnormal combustion scenarios like hot-spot induced pre-ignition [11]. Recent research has identified novel flame physics and regimes under elevated temperatures, including cool flame [12], warm flame [13], autoignition-assisted flame [14], and thermal pyrolysis induced overdriven flame [15]. Some of these phenomena are systematically reviewed by Ju and coworkers recently [16,17].

* Corresponding author.
E-mail address: pzhao12@utk.edu (P. Zhao).

https://doi.org/10.1016/j.combustflame.2021.111765
0010-2180/

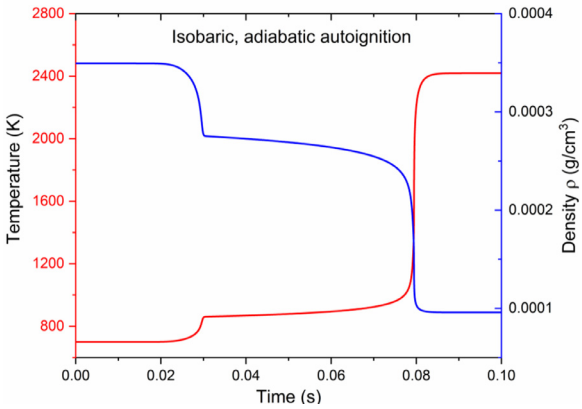

Fig. 1. Evolution of temperature and density for the isobaric adiabatic ignition of the target mixture n-heptane/O_2/N_2/He (18% O_2, 41% N_2, 41% He by mole).

A major physical effect expected from elevated unburnt mixture temperature is the inevitable non-zero reaction progress from autoignition and/or thermal pyrolysis chemistry in the immediate upstream of a flame, especially for large hydrocarbon and oxygenated fuels exhibiting pronounced low-temperature chemistry and two-stage ignition [18]. With partially reactive nature of such mixture under elevated temperature conditions, reaction progress can further accumulate as combustion evolves, leading to substantial thermal and chemical changes in the reformed mixture directly entering the flame structure. From combustion theory, this is by nature a severe cold-boundary difficulty [19] that cannot be ignored with the intrinsic coupling of flame and upstream reaction progress under elevated temperature. Due to the complexity and experimental challenge of this problem, previous relevant studies are mostly computational [14,20–25]. For example, in a recent work [25], it is found that the flame speed can be increased up to 100% or higher with increasing reaction progress, and a reduced mixture strategy is developed to capture the flame speed under autoignition conditions.

Only until very recently, it becomes feasible to experimentally investigate high-temperature laminar flames in a shock tube with well-controlled thermodynamic conditions [26–29]. Hanson and coworkers innovatively integrated systems of laser ignition system and chemiluminescence capture to the test section of a regular shock tube. As such, laminar flames can be initiated at the desired thermodynamic conditions induced by the reflective shock, and at the desired extent of chemical reaction progress during autoignition [29]. Good consistency has been achieved with previous experimental data and kinetic modeling reported in the literature, especially for simple fuels such as methane and propane [26]. However, relative larger amount of scatter is observed in the shock tube flame experiment for large hydrocarbon fuels such as n-heptane and isooctane [27,28]. Furthermore, wrinkling and distortion of flames have been observed for these fuels, which have added more ambiguity to the interpretation of the experimental results. To gain more insights into these new and valuable experimental targets, recent simulation by Yang et al. [15] have identified a novel pyrolysis induced overdriven flame during flame evolution, which can successfully explain the observed non-monotonicity in isooctane flame speed in the intermediate temperature regime. For n-heptane with higher reactivity, Zhang et al. [30] have shown the potential role of double flame in the observed non-monotonicity in the n-heptane flame speed, by simulation in a 1-D spherical constant volume configuration. However, given the coupled complexities of flame stretch, flame front instability, upstream chemical reactivity, shock-induced flow, and flame transition, it adds to substantial challenges to fully understand the experimental data and guide future experiments.

To completely understand the features of flame initiation and propagation under high temperatures, the current work conducts transient and steady simulation of the simplest flame configuration – 1D planar flames with detailed chemistry and transport, for the mixture and thermodynamic conditions similar to the Stanford shock tube experiment [29]. Given the absence of flame stretch, this study focuses on the thermal-chemical effects of reaction progress on flame initiation and propagation. First, a range of ignition energy has been applied to identify the regime and features of flames that can be initiated at elevated temperatures; secondly, ignition timing - the instant when ignition energy is applied has been varied to demonstrate the effects of unburnt reaction progress on the subsequent flame initiation; thirdly, by comparing the steady and unsteady solution of the flames, sensitivity and time scale analysis are further conducted on the steady-state flame to understand the controlling thermal chemical characteristics of these flames. Flame regime transition is analyzed to provide insights into future experiments and for general high-temperature combustion control.

2. Numerical model and methodology

In the present study, the numerical simulation is conducted using the in-house reacting flow platform reactingFOAM-SCT based on OpenFOAM 6.0, which solves the Navier-Stokes equations together with the species and energy conservation with detailed chemistry and transport by incorporating recent advances in computational combustion. The accuracy and performance of reactingFOAM-SCT are systematically validated against DNS results or analytical solutions in different configurations, including ignition delay, shock and expansion fan, diffusion-convection process, 1D spherical flame initiation and propagation, 1D non-premixed counterflow flame, 2D premixed flame instabilities, 2D non-premixed co-flow flame [31]. More recently, this computational platform has been utilized to investigate cool flame initiation [12], autoignition and reaction front dynamics in stratified mixtures [32], high-temperature flame initiation and propagation [15], two-stage ignition in a laminar boundary layer [33], etc.

The unsteady simulation adopts a 1-D planar computational domain with a length of 5.75 cm. Uniform grid of 10 μm is employed across the whole region to resolve the flame initiation and propagation, which is also justified by additional grid independence study. The maximum CFL number is set to be 0.4 to control the integration time step and ensure convergence. Zero-gradient and symmetry boundary condition are imposed on both inner (x = 0 cm) and outer (x = 5.75 cm) boundaries, respectively. To avoid growing acoustic waves and achieve nearly constant-pressure environments, a wave transmissive boundary condition is applied at the outer boundary. Initially, a static homogeneous n-heptane/O_2/N_2/He (18% O_2, 41% N_2, 41% He by mole) mixture with equivalence ratio of 0.9 fills the domain, at a temperature of 700 K and pressure of 1 atm, close to the experiment. Following [15], the flame initiation is achieved by heat deposition from a hot spot, which is described by an extra source term with a time and spatial dependence in the energy conservation equation:

$$\dot{q}_{ig} = \begin{cases} \frac{E_{ig}}{\frac{4\pi}{3} x_{ig}^3 \tau_{ig}} exp\left[-\left(\frac{x}{x_{ig}}\right)^8\right] & 0 \le t - t_{ig} < \tau_{ig} \\ 0 & t - t_{ig} \ge \tau_{ig} \end{cases}$$

where E_{ig} is the total ignition energy, τ_{ig} is the duration of the energy source, and x_{ig} is the ignition kernel size. Following [15], the duration time and ignition kernel are set as constant with τ_{ig} = 50 μs and x_{ig} = 2 mm, respectively, t_{ig} is the ignition timing, when ignition energy starts to be deposited.

In the computation, ignition energy is varied from 1 mJ to 100 mJ to observe the subsequent flame evolution and regimes. Given the elevated temperature and chemical reactivity, two-stage ignition is expected to occur in the mixture, with the adiabatic, isobaric first-stage ignition delay τ_1 controlled by the low temperature chemistry and identified by local maximum temperature rise rate. To characterize the reaction progress in the unburnt mixture during flame initiation and propagation, a dimensionless residence time is defined as time normalized by the first-stage ignition delay, i.e., t/τ_1 where $\tau_1 = 29.73$ ms as in Fig. 1. In the case of steady and unsteady flame propagation, this dimensionless time also can be referred to as the ignition Damköhler number (Da) in the upstream unburnt mixture, for example, as used in [13,30]. This dimensionless residence time is also used to indicate the 'dimensionless ignition timing' when the ignition energy starts to be deposited, i.e., t_{ig}/τ_1. In addition to the baseline with dimensionless ignition timing of 0, ignition timing is varied below unity to trigger a flame prior to the first-stage ignition delay, as well as above unity values to trigger flames in mixtures reformed by the low temperature chemistry. For data post-processing, the flame front X_f is identified by tracking the position with local peak heat release rate and the burned flame propagation speed S_b can be obtained by $S_b = dX_f/dt$.

For 1D steady planar premixed flame simulation, the ANSYS Chemkin-Pro-V2020 R1 with detailed chemistry and mixture-average transport model is utilized to calculate the steady laminar premixed flame propagating into the partially reactive mixtures prior to or after the first-stage auto-ignition. Both the adaptive mesh criteria – GRAD and CURV are both set to 0.01 so that more than 1000 grids points are included in the converged flame structure. This can guarantee the grid independence of laminar flame speed. At each running case, the upstream domain length is gradually decreased to the shortest values so that the relative error of the flame speed can be less than 10^{-4} to ensure the flame front is independent of domain size. The instantaneous thermodynamic condition and chemical composition is adopted from the homogeneous adiabatic isobaric ignition data (Fig. 1) at different reaction progress to produce the partially oxidized mixtures as the inlet boundary conditions of a premixed flame.

A detailed mechanism for n-heptane including 135 species and 651 reactions [34] has been utilized in this work, where the thermal and transport properties of helium are obtained from the kinetic mechanism [35]. Further mechanism validation can be found in the Supplemental materials, which demonstrates the Andre 2013 mechanism can well capture the ignition delay time and laminar flame speed under a wide range of conditions. It should be noted that although the thermodynamic condition in the current study is limited to 1 atm and 700 K, the results can provide general insights to flame initiation and propagation for arbitrary fuels with low temperature chemistry in the NTC regime. With further increased temperature beyond NTC, for example 1000 K under 2 atm for the same mixture, the effect of low temperature will be absent, and the ignition will become a single stage. Such a problem is less challenging and can be addressed using the same method and analysis in the current work.

3. Results and discussion

3.1. Unsteady flame initiation and propagation

3.1.1. Overall flame regimes and behaviors at $t_{ig}/\tau_1 = 0$: hot and cool flames

Our recent work has shown that for DME/air mixtures at elevated temperature, it is possible to directly initiate cool flames when ignition energy is below the minimum ignition energy (MIE) of conventional hot flames [12]. To understand the overall regimes of flame initiation and propagation regimes, an ignition energy sweep is first performed for the current n-heptane/air/He mixture under the targeted conditions $P = 1$ atm, ϕ=0.9, $T = 700$ K. As baseline, ignition energy is deposited at $t_{ig} = 0$ s, i.e., the dimensionless ignition timing is $t_{ig}/\tau_1 = 0$. Fig. 2 shows the flame front position evolution for ignition energy from 1 mJ to 100 mJ. Two distinct regimes have been found – both hot flames with fast propagation and cool flames with much slower propagation. It is seen that hot flames can be directly initiated after a certain period of induction time, when ignition energy is higher than 7 mJ. In this regime, a hot flame can be triggered faster with higher ignition energy. When the ignition energy is around 20 mJ or higher, the hot flame trajectories tend to collapse in the time range of interest, indicating that a flame will be initiated almost immediately regardless of the ignition energy. On the other hand, for ignition energy below the 7 mJ, instead of ignition failure, cool flames can be initiated with a much longer induction time and much slower propagation. When ignition energy is approaching 6.8 mJ, cool flame onset is advanced to 0.02 s, which is the shortest induction time for cool flame initiation, and still much longer than hot flame initiation. It is worth noting that for all cool flames, flame evolution regime of interest is before the first-stage ignition delay. Here we select the four lower ignition energies at 6.8 mJ, 5.8 mJ, 5.4 mJ, and 4 mJ to illustrate the cool flame initiation and propagation characteristics.

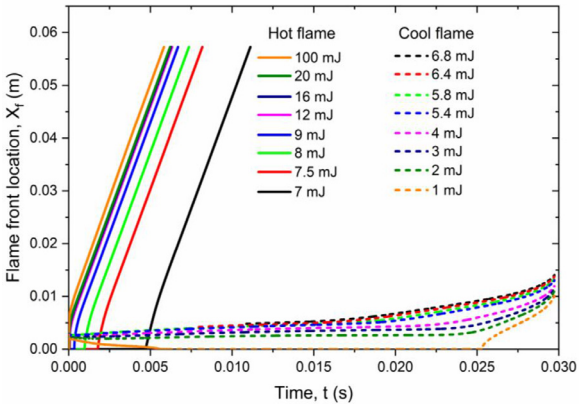

Fig. 2. Evolution of flame front position with various ignition energies for n-heptane/air/He mixture at $P = 1$ atm, ϕ =0.9, $T = 700$ K, showing regimes for both cool and hot flames.

Figs. 3(a)-(b) show the flame front position X_f vs. time t and burned flame speed S_b vs. reaction progress for cool flame regimes. Due to the much longer induction time of these cool flames, the reaction progress in the unburnt mixture eventually approaches unity toward the first-stage ignition. Consequently, these cool flames are essentially autoignition-assisted cool flames. Unlike the eventually collapsed hot flames, these autoignition-assisted cool flames strongly depends on the ignition energy even at the same upstream reaction progress, before the first-stage ignition occurs. In other words, the dynamics of autoignition-assisted cool flames sensitively depends on the initiation trajectory even for the same reaction progress in the unburnt mixture. As shown in Fig. 3(b), before reaching the plateau, a cool flame front creeps very slow, controlled by the ignition kernel development and diffusion; when the unburnt reaction progress reaches about 0.6 or higher, a sudden acceleration occurs and then a self-sustained cool flame forms and stays on a plateau with nearly quasi-steady propagation. Until reaction progress reaches 0.8 or higher, a very strong acceleration occurs accompanying the first-stage ignition. Therefore, cool flame propagation includes a period of quasi-steady propagation (i.e., the plateau) follows by a strong autoignition driven acceleration when reaction progress approaches unity. Also, although the 6.8 mJ case

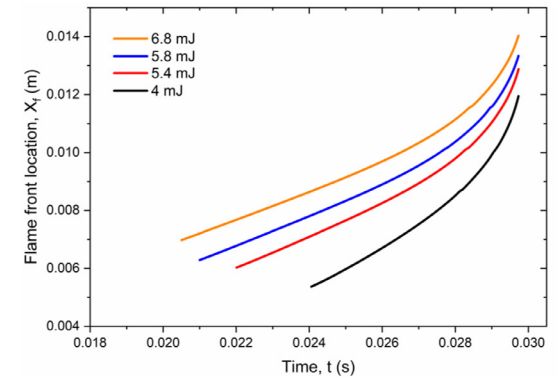

(a)

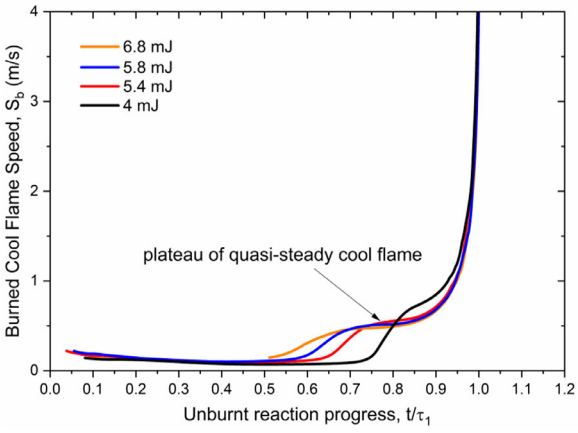

(b)

Fig. 3. (a) Flame front position X_f vs. time t; (b) Burned flame speed S_b vs. unburnt reaction progress, t/τ_1 for cool flame initiation & propagation under E_{ig} = 6.8, 5.8, 5.4 and 4 mJ.

initiates a cool flame earlier, the propagation velocity of the corresponding cool flame is the lowest among all the ignition energies; the 4 mJ case initiates a cool flame the latest, the cool flame propagation velocity is the fastest, at the same unburnt reaction progress of 0.85. As the first stage autoignition occurs at 29.73 ms, the cool flame speeds sharply increase and overlap on the S_b vs. Da plot due to the nearly instantaneous heat release in the unburnt mixture.

To illustrate flame propagation acceleration characteristics with increasing unburnt reaction progress, three instants at E_{ig} = 5.8 mJ are selected along cool flame evolution to further demonstrate the thermal-chemical structures of different cool flame structures. Instant 1 at 0.02343 s (reaction progress t/τ_1= 0.79) denoting the normal cool flame with minor autoignition effect right on the plateau; Instant 2 at 0.02619 s (reaction progress t/τ_1= 0.88) with immediate autoignition effect toward the end of the plateau; Instant 3 at 0.02932 s (reaction progress t/τ_1= 0.99) at a later stage right before autoignition effect takes over. As shown in Fig. 4, it is observed that the unburnt temperature of Instant 1 stays around 700 K, while it increases by 20 K for Instant 2 with the autoignition assisted effects. Meanwhile, apparent increase of low temperature chemistry products CO, CH_2O, and H_2O_2 is seen within the flame. At Instant 3, the unburnt temperature rises by 80 K, and the peak cool flame temperature increases by 30 K. Substantial consumption of n-C_7H_{16}, O_2 and production of low temperature products are further observed. These changes in the thermal-chemical

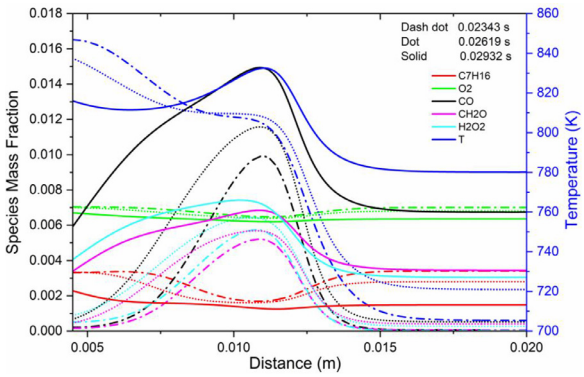

Fig. 4. Comparisons of the thermal-chemical structures of regular cool flame and auto-ignited cool flame under three different instants.

structure of different types of cool flames demonstrates the critical role of unburnt mixture reaction progress.

3.1.2. *Flame initiation with varying ignition timing* t_{ig}/τ_1

Given the fast flame initiation and propagation, negligible unburnt reaction progress is involved in the baseline hot flame cases. For example, the 7 mJ ignition energy case with longest time for flame propagation corresponds to a final unburnt reaction progress around 0.3. As such, the effect of unburnt mixture reaction progress is nearly negligible on hot flame initiation and propagation. In this section, we fix the ignition energy at 20 mJ, and change the ignition timing before or after the first-stage ignition to explore the flame initiation and propagation features with varying extent of unburnt reaction progress. With 20 mJ ignition energy, the hot flame initiation is almost immediate, in the order of 0.01 ms. As expected, with delayed ignition for dimensionless ignition timing t_{ig}/τ_1 from 0.88 to 0.98, the remaining delay time to the first-stage ignition will be further shortened. Therefore, we can expect the occurrence of first-stage ignition during the hot flame propagation, such that the changes in flame properties can be investigated when the unburnt mixture is reformed by the low-temperature chemistry.

Fig. 5(a)-(b) show the burned flame speed S_b vs. X_f for dimensionless ignition timing both less and greater than unity, including t_{ig}/τ_1 = 0.88, 0.94, 0.96, 0.98 and 1.2, 1.4 and 1.6 respectively. It can be observed that there is a clear bump in the flame speed during the flame propagation processes, induced by the first-stage ignition. This is because, as autoignition occurs, substantial thermal expansion is induced by volumetric heat release in the unburnt mixture ahead of the hot flame, which causes increased upstream flow velocity and in turn leads to the observed increment in burnt flame speed. At the location with peak autoignition heat release, effects from thermal expansion are the strongest. As ignition finishes, the ignition heat release rate decreases to zero. Consequently, thermal expansion disappears, and a uniform unburnt velocity profile is restored. Another interesting phenomenon is that for delayed ignition timing, the bump will appear sooner and leave a longer distance for the hot flame propagation in the post first-stage ignition, low-temperature chemistry reformed products. After the occurrence of first-stage ignition, all flames initiated at different ignition timing collapse on the S_b vs. X_f plots and exhibit the same S_b. The results suggest that as long as the first-stage ignition has already occurred in an unburnt mixture, hot flames tend to have the same flame speed, completely forgetting about the historical effects before the first-stage ignition. Also, an increase in S_b is observed across the bump due to the thermal-chemical effects of the low temperature chemistry, similar to [23,25].

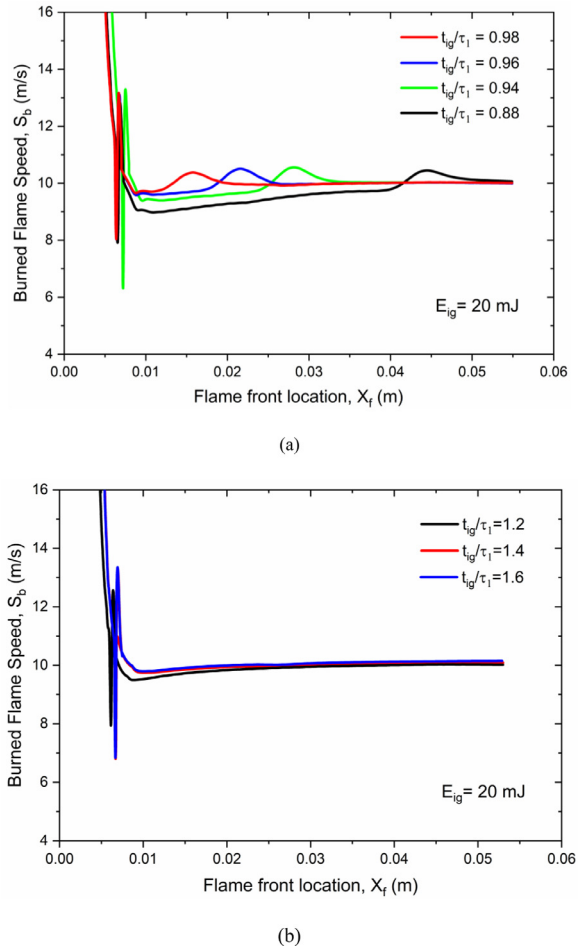

Fig. 5. Burned flame speed S_b vs. X_f for auto-ignited hot flame initiation at dimensionless ignition timing t_{ig}/τ_1 = (a) 0.88–0.98 (b) 1.2–1.6, with E_{ig} = 20 mJ.

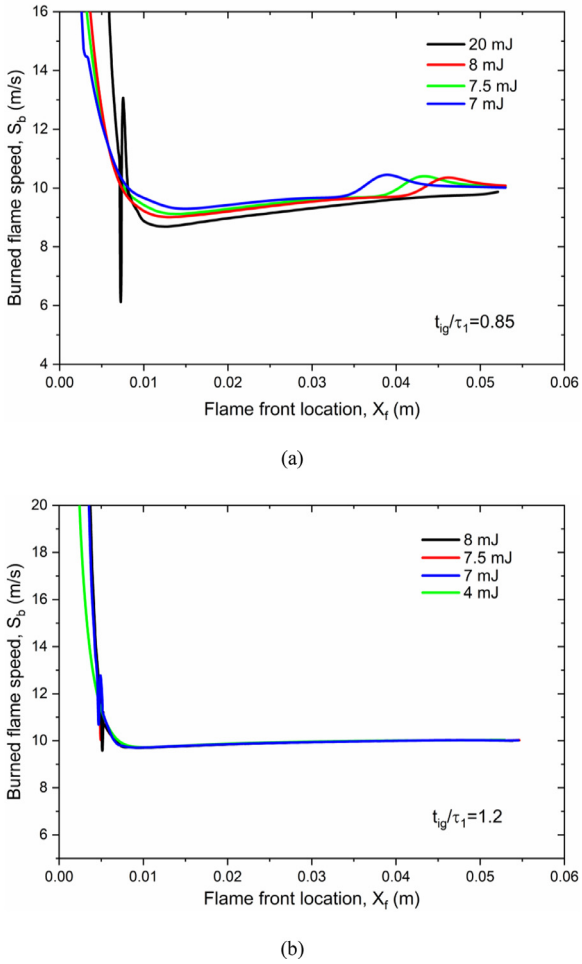

Fig. 6. Burned flame speed Sb vs. X_f for auto-ignited hot flame initiation for various ignition energies at dimensionless ignition timing t_{ig}/τ_1 of (a) 0.85 and (b) 1.2.

3.1.3. Flame initiation for non-zero unburnt reaction progress with varying ignition energy

As the ignition energy plays a key role to trigger different flame regimes, we further investigate the flame initiation and propagation features under given unburnt reaction progress with varying ignition energy, before and after the first-stage auto-ignition. Fig. 6(a)-(b) show the flame front position burned flame speed S_b vs. X_f with ignition energy from 4 to 8 mJ at fixed dimensionless ignition timing t_{ig}/τ_1 at 0.85 and 1.2. For the t_{ig}/τ_1 = 0.85 cases, it is seen that obvious first-stage autoignition occurs for the three lower ignition energy cases, while the 20 mJ case does not allow sufficient residence time for the first-stage ignition to occur, given the faster flame induction. Before the first-stage ignition occurs, the lower ignition energy cases tend to induce higher flame speed. It is hence emphasized that due to the differences in flame induction timing, these cases do not overlap in the S_b vs. X_f phase plot, causing greater difficulties in define and compare flame data.

However, for the t_{ig}/τ_1 = 1.2 cases, it can be observed that, there exhibits negligible difference in the flame induction time, and the flame front trajectories and phase evolution largely overlap as well. When further reducing the ignition energy to 4 mJ, under which condition a hot flame cannot be initiated in the baseline cases as shown in Fig. 2, a hot flame can nevertheless be successfully triggered for the current case at delayed ignition timing t_{ig}/τ_1 of 1.2. This indicates that the mixture reactivity is dramatically enhanced after the first-stage autoignition, such that a hot flame can be triggered more easily. Overall, the results here suggest that with unburnt reaction progress beyond first-stage ignition, flame induction time becomes very insensitive to ignition energy. As such, flames can be triggered in a more reliable manner. The enhanced mixture reactivity further reduces the minimum ignition energy and extends the regime for hot flame initiation.

3.1.4. Observation of double flames

Double flame is an interesting flame regime including both cool and hot flame fronts during combustion evolution under elevated thermodynamic conditions, for fuels exhibiting NTC behaviors [30,36–38]. Depending on if the cool or hot flame front appears first, there can be two mechanisms for the formation of a double flame. One scenario is starting from a hot flame, with a cool flame gradually splitting from the preheat zone, and thereby forming a double flame structure [38]. On the contrary, the other type is starting from a cool flame, with a hot flame eventually established in the downstream [36]. Chemiluminescence images from the shock tube flame experiment [29] also show the multilayer flame structures under autoignitive conditions, implying the potential relevance of double flames. In the current isobaric planar flame simulation, we have also observed these two cool flame formation mechanisms, although they are quite mild and highly transient, as such do not obviously affect the flame speed and regimes.

Fig. 7 shows the thermal-chemistry structure of a typical double flame. It can be observed that the double flame structure consists of a leading cool flame and a trailing hot flame. The leading cool flame front generates low temperature products such as

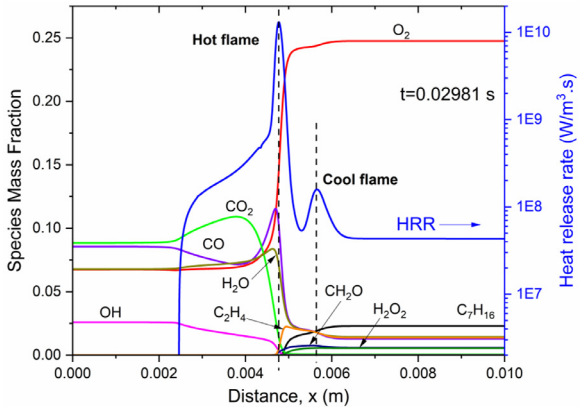

Fig. 7. Thermal-chemical structure of a double flame at $t = 29.81$ ms in the case with ignition energy 20 mJ and dimensionless ignition timing t_{ig}/τ_1 around 1.0.

CO, CH_2O, H_2O_2 and further feeds these species to the trailing hot flame, where more complete oxidation occurs and produces large amounts of CO_2, H_2O and heat. As this is still in the initial stage of flame initiation, high concentration of CO remains in the downstream of the hot flame. Double peaks are shown in the heat release rate profile, where the peak from the hot flame segment is about two orders of magnitude higher than that of the cool flame. Therefore, we can track the locations of both local peaks in the heat release rate profiles to show the evolution of the double flames.

Fig. 8(a) shows the evolution of the first type of double flame that occurs in the case with ignition energy 20 mJ and dimensionless ignition timing t_{ig}/τ_1 of 1.0. Initially, a hot flame is directly triggered. Shortly after at $t = 29.75$ ms, a faster propagating cool flame is split from the base of the hot flame generating a double flame structure consisting of a leading cool flame and a trailing hot flame. As the first-stage ignition completes, burning intensity of the cool flame gradually decays. Eventually, the trailing hot flame catches up with the cool flame front and merges with it at 0.03001 s. In fact, the double flame in this case is closely coupled and completely separated as opposite to the scenarios where an obvious plateau can appear in the temperature profile [38]. The double flame in this case can be referred to as "hot flame induced double flame", which only lasts about 0.26 ms, as such it plays negligible role in the subsequent flame propagation.

Another type of double flame, the cool flame induced double flame, is shown in Fig. 8(b). Different from the previous category splitting from a hot flame, the second type of double flame starts with a cool flame at $t = 0.02547$ s, and then a hot flame is formed $t = 0.02667$ s in the downstream of the leading cool flame by high temperature autoignition. It is interesting to be seen that there is a turning point in the cool flame trajectories when the hot flame is initiated, as shown by the steeper slope in Fig. 8(b). This is due to the strong thermal expansion by the downstream hot flame initiation, which further pushes the cool flame to move forward. In the meantime, the leading cool flame feeds low temperature chemistry reformed products including CH_2O, CO, etc., to the hot flame, which in turn facilities its propagation. Unlike the hot flame induced double flame shown in Fig. 8(a), the cool flame burning intensity remains constant during its propagation process with a heat release rate about 2×10^7 W/m^3. While the hot flame has a release rate around 1×10^{10} W/m^3, about three orders of magnitude higher than that of the cool flame. The hot flame has a much higher speed and eventually swallows the leading cool flame after a co-existing period about 0.4 ms. It is seen that the cool flame induced double flame can appear in wider ranges of ignition timing with sufficiently low ignition energies.

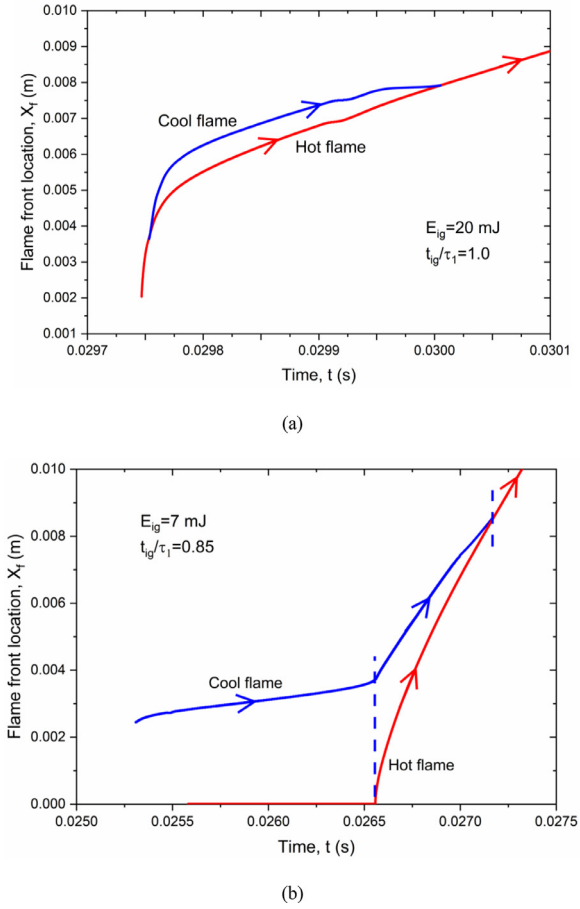

Fig. 8. (a) Double flame mode 1: Hot flame induced cool flame at t_{ig}/τ_1=1.0 and $E_{ig} = 20$ mJ; (b) Double flame mode 2: Cool flame induced hot flame at $t_{ig}/\tau_1 = 0.85$ and $E_{ig} = 7$ mJ.

3.2. Comparison with quasi-steady flames in partially reactive mixture

Due to the partially reactive nature of the unburnt mixture at $T_u = 700$ K, it is not a trivial practice to obtain the steady laminar premixed flame solution in the classical diffusion-reaction limit. Our goal is to seek an adequately refined laminar premix flame, whose structure and propagation property is independent of computational domain, and meanwhile, whose burning flux is the eigenvalue of the governing equations for the desired intermediate mixture. The following procedures are hence adopted to obtain such a solution. First, the instantaneous mixture composition is sampled at the desired reaction progress t/τ_1 during the homogenous adiabatic, isobaric autoignition process, which serves the upstream inlet mixture for the flame. Secondly, continuation studies are performed to show the dependence of the flame property on the computational domain. As shown in Fig. 9(a), for a typical partially reactive mixture at reaction progress of 0.92, the flame speed only converges at sufficiently short upstream domain length e.g., below 0.1 cm, to avoid the effects of autoignition. With sufficiently reduced upstream, flame thickness $\delta = (T_b\text{-}T_u)/\max(dT/dx)$, flame integration time scale $\int^d x/u$ from inlet to flame front, and the flame characteristic time scale δ/S_u all tend to converge. With increasing upstream domain, the flame speed substantially increases and eventually exponentially depends on the domain as it reaches the spontaneous propagation limit. Furthermore, the downstream domain length has to be sufficiently long to ensure the chemical equilibrium and adiabatic flame temperature T_b is reached, as

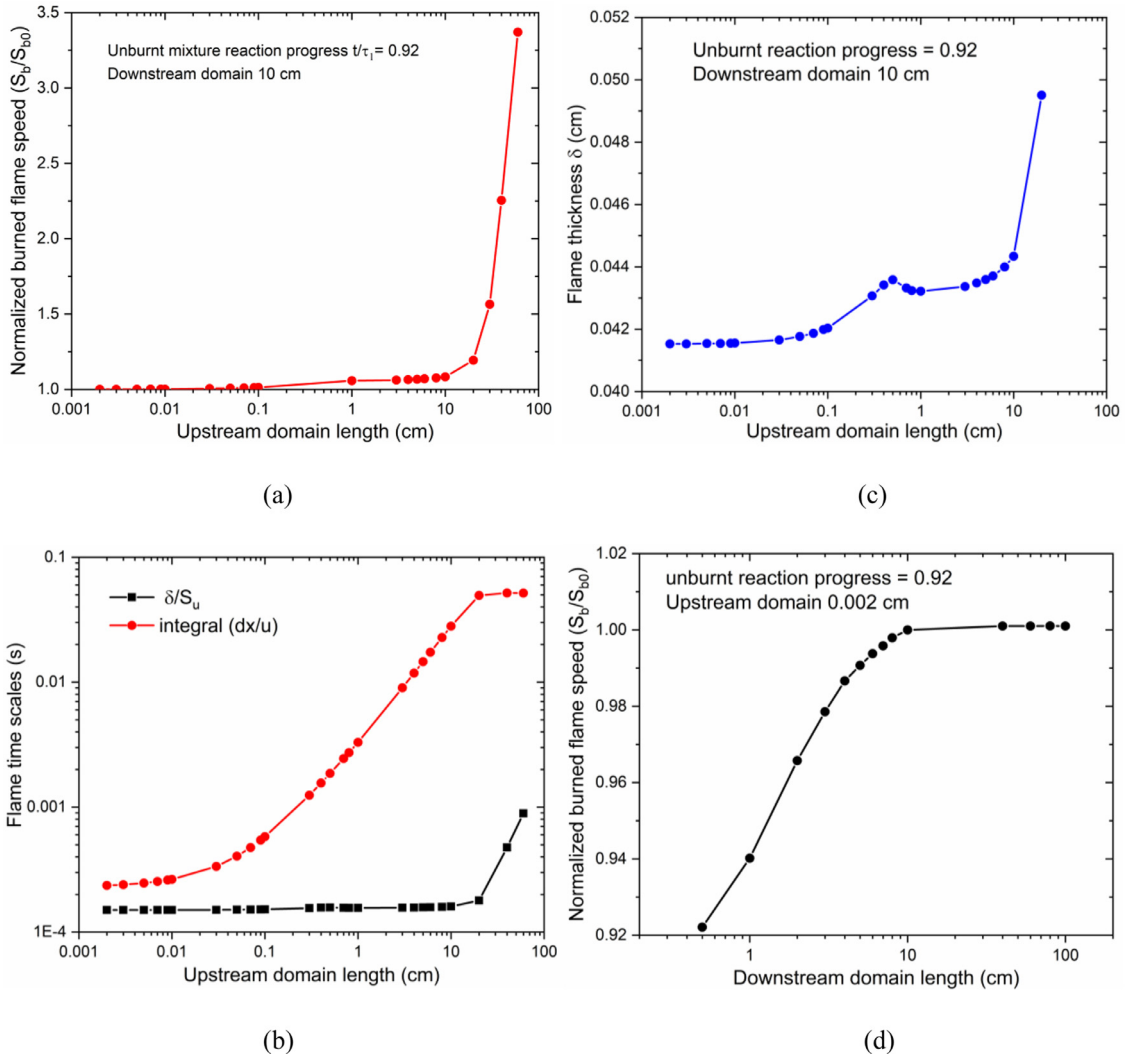

Fig. 9. (a) Dimensionless burned flame speed S_b/S_{b0} as a function of the upstream domain size and (b) flame time scales as a function of upstream domain length (c) flame thickness as a function of upstream domain length (d) Dimensionless burned flame speed S_b/S_{b0} as a function of downstream domain length, for steady premix flames with inlet unburnt mixture reaction progress t/τ_1=0.92.

shown in Fig. 9(d). Meanwhile, a solution should satisfy the zero-gradient conditions at both upstream and downstream boundaries. Therefore, a well-defined steady laminar premixed flame solution can only be obtained with sufficiently short upstream and sufficiently long downstream domain.

Fig. 10 compares the unsteady and steady flame speeds and summarizes the burned flame speed as a function of unburnt reaction progress t/τ_1. Good quantitative agreement has been achieved between the steady and unsteady solutions, indicating that the unsteady flame propagates in a quasi-steady manner in the diffusion-reaction limit. It can be observed that the flame experiences three different regimes when the same ignition energy is applied at varying ignition timing. For sufficiently small unburnt reaction progress, $0 < t/\tau_1 < 0.7$, flame propagation is weakly assisted by autoignition as such the burning velocity is about 8.4 m/s and remains insensitive to the increasing unburnt reaction progress. For sufficiently high unburnt reaction progress, t/τ_1 of 1 or higher, the first-stage ignition has already occurred during the hot flame initiation, leading to enhanced unburnt mixture reactivity and the temperature, as such the burnt flame speed is increased to a constant value around 10 m/s. This is a regime where the flame propagation is strongly assisted by autoignition, and the flame speed is also insensitive to the reaction progress in the post first-stage ignition mixture. Transitions between these two regimes will occur with intermediate unburnt reaction progress, $0.7 < t/\tau_1 < 1$, where the flame speed is highly sensitive with ignition timing prior to the first-stage ignition, and stays around 10 m/s afterwards. Therefore, extra caution should be taken for hot flame experiment in the transition regime.

Given the varying effects of ignition products on flame propagation, we have selected the more refined steady-state premixed flame solution to further investigate the time scales, scaling laws and controlling chemical reactions for these autoignition assisted flames. Fig. 11 demonstrates the comparison of flame and ignition time scales for the steady state flames in the diffusion-reaction limit. τ_{flame} is the characteristic flame time δ/S_u, τ_{chem} is the remaining time relative to the closest ignition event. For reaction progress $t/\tau_1 < 1$, τ_{chem} refers to the remaining delay time to the first-stage ignition for the unburnt mixture; for $t/\tau_1 > 1$, τ_{chem} refers to the remaining delay time to the main ignition. As long as the reaction progress t/τ_1 is away from unity, the steady solution always allows a much shorter flame time scale compared with the chemistry time scale. In other words, the ratio $\tau_{\text{flame}}/\tau_{\text{chem}}$ is always far less than unity, to ensure ignition is absent within the flame structure, which is an important criterion to justify the steady-state flame solution. When $\tau_{\text{flame}}/\tau_{\text{chem}}$ be-

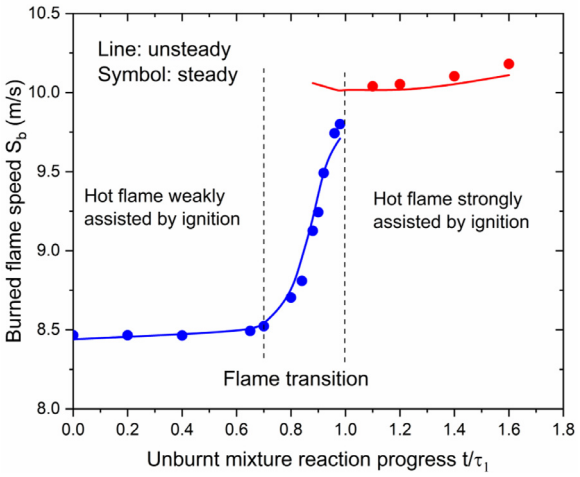

Fig. 10. Comparisons of the steady and unsteady burned flame speed S_b as a function of unburnt mixture reaction progress t/τ_1 demonstrating the quasi-steady propagation and flame transition with increasing reaction progress.

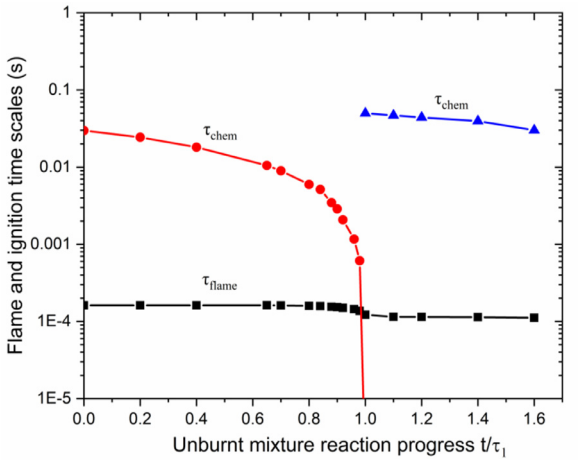

Fig. 11. Flame and chemistry time scales as a function of unburnt mixture reaction progress t/τ_1.

comes order unity, transient effects from autoignition become non-negligible, such as the "bump" in flame speed induced by pressure disturbance when the first-stage ignition occurs. Under other thermodynamic conditions, we have observed substantial deceleration even back propagation as the flame is pushed by the pressure disturbance before eventually transitioning to an autoignitive reaction front from the unburnt mixture autoignition. In general, as autoignition delay is close to the flame propagation time scale, the interaction of pressure wave and flame becomes significant, and the phenomenon becomes highly transient. Our previous relevant studies [22,39] have suggested interaction of autoignition and flame is highly case by case, and can be usually classified using the detonation peninsula theory proposed by Bradley [40,41].

To demonstrate the generality of quasi-steadiness, in addition to the current set of unburnt condition, we have so far investigated transient flame initiation and propagation for n-heptane, DME and propane (all exhibit NTC) under a wide range of thermodynamic conditions. Based on our observation, as long as the remaining autoignition delay to the first-stage or the main ignition event is much longer than the characteristic flame time ($\tau_{chem}/\tau_{flame}>>1$), the unsteady effect during flame propagation is negligible, as there is negligible involvement of acoustic waves and pressure fluctuations, the flame in general propagates quasi-steadily in a partially reacting mixture both prior-to or post the first-stage ignition. Such observations are justified by the comparison of steady and unsteady flame solutions, as well as budget term analysis from convection, diffusion and reaction terms in the transient solution, showing negligible magnitude of the unsteady terms.

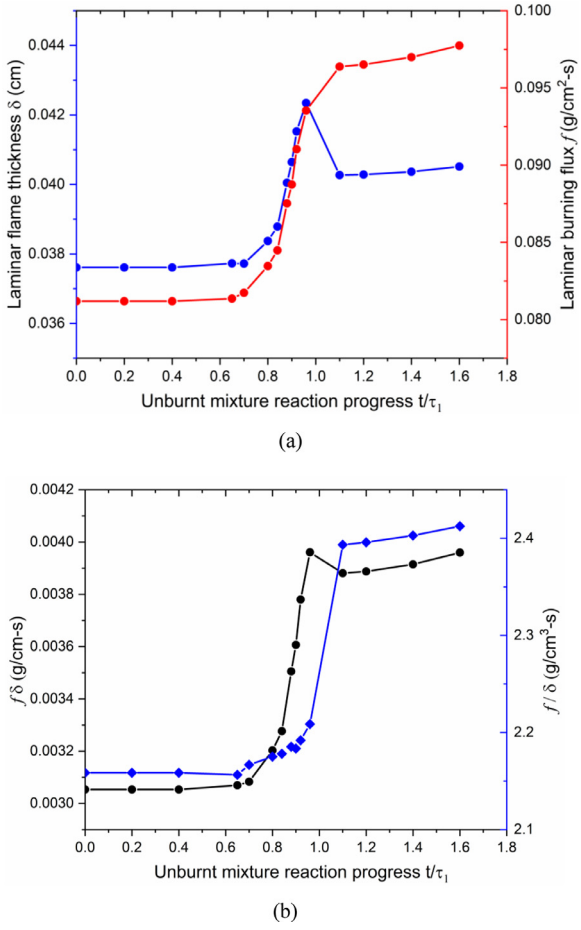

Fig. 12. (a) Laminar burning flux f and laminar flame thickness δ (b) the product $f\,\delta$ and ratio f/δ as a function of unburnt mixture reaction progress.

Another two important flame properties are further evaluated at different upstream reaction progress. The first one is the flame thickness δ, which is a unique flame length scale and key scaling parameter in turbulent combustion. The other one is the laminar burning flux f, eigenvalue of the species and conservation equation. In the laminar flame theory, simple scaling rules can be obtained using f and δ, by recognizing the dominant balance between convection and diffusion in the preheat zone, as well as the reaction-diffusion balance in the reaction zone. For example, it can be shown that $f\,\delta \propto \lambda/c_p$ only depends on the transport parameter, while $f/\delta \propto \omega/Ze$, the ratio of reaction rate and the Zel'dovich number Ze. As shown in Fig. 12, for upstream mixture far prior to the first-stage ignition, i.e., $t/\tau_1 < 0.7$, or post the first-stage ignition ($t/\tau_1 > 1.0$), both the laminar flame thickness and burning flux exhibit negligible change with variation in upstream mixture reaction progress, however, compared with upstream mixture prior to the first-stage ignition, laminar burning flux f increases by nearly 20% and the laminar flame thickness δ increases by about 5% in the post first-stage mixture. By plotting both the product and ratio of f and δ with varying upstream mixture reaction progress, it can be seen that $f\,\delta$ and f/δ are still invariants for mixtures either far prior to or post the first-stage ignition, but corresponding to different values. Overall, it can be concluded that the post first-stage ignition mixture has a stronger facilitation effect for flame propagation, allowing faster flame speed, thicker flame structure

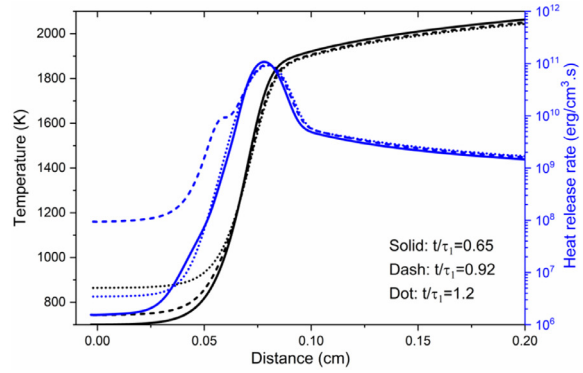

(a)

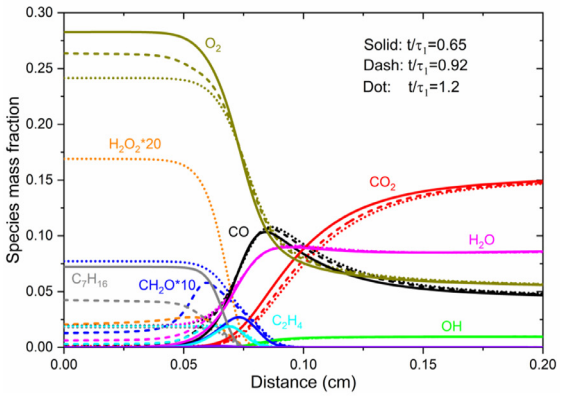

(b)

Fig. 13. Comparison of (a) thermal (b) chemical structures of steady premixed flames with three mixtures of different unburnt reaction progress before or after the first-stage ignition.

and higher burning flux. This is a combined thermal-chemical effect including the contribution from both elevated temperature and mixture composition reformed by the low-temperature chemistry.

Fig. 13 shows the comparison of thermal and chemical structures of autoignition assisted flames at three different unburnt reaction progress before or after the first-stage ignition. As expected, these flames have different upstream temperature, unburnt composition and heat release rate, they nevertheless should always share the same adiabatic flame temperature. As t/τ_1 increases, concentration of n-heptane and O_2 keep decreasing, and the amount of intermediates including CH_2O, C_2H_4, and H_2O_2 keeps increasing in the upstream unburnt composition. Regardless of such differences, the profiles of major products downstream of the flame are largely similar, including H_2O, CO_2, CO, and OH. It is therefore of interest to identify the key reactions that affect the flame speed with different unburnt reaction progress.

Results of global sensitivity analysis (SA) on the most important reactions are listed in the supplementary material for the steady-state laminar premixed flames at $t/\tau_1 = 0.65$, 0.92 and 1.2. 10% perturbation is introduced on the A factor of the corresponding reaction to calculate the logarithmic sensitivity coefficient (LSC): $LSC = A_i/S_u^*(\Delta S_u/\Delta A_i)$. Given the strong role of ignition played in these flames, the flames before perturbation are obtained with sufficiently short upstream and sufficiently long downstream domain, in the classical diffusion-reaction limit. After the perturbation on a certain A factor is introduced, flame and chemistry time scales are further examined in the flame, to ensure the ratio τ_{flame}/τ_{chem} is far less than unity, as listed in the last column of the tables in the supplementary material. This is important to ensure the effect from ignition is decoupled from the evaluation of key reactions to the flame propagation. The top 10 most important sensitive reactions that promoting and retarding flame propagation are selected respectively with their LSC shown in Fig. 14. It is interesting to observe that the most important reactions facilitating flame propagation include $H + O_2 = O+OH$, $CO+OH = CO_2+H$ consistent with our understanding on regular laminar flames [42]. No low temperature pathway is explicitly seen from the sensitivity calculations, different from the sensitivity analysis performed in [22] with very long upstream domain, where the effect on ignition dynamics and flame propagation is not appropriately decoupled. However, it is certainly not correct to claim low temperature chemistry is not important in these flame speed. The reason is two-fold: on one hand, low temperature fuel reforming and chain branching substantially affects the chemical composition entering the flame structure, and such they are intrinsically needed to determine the flame speed;

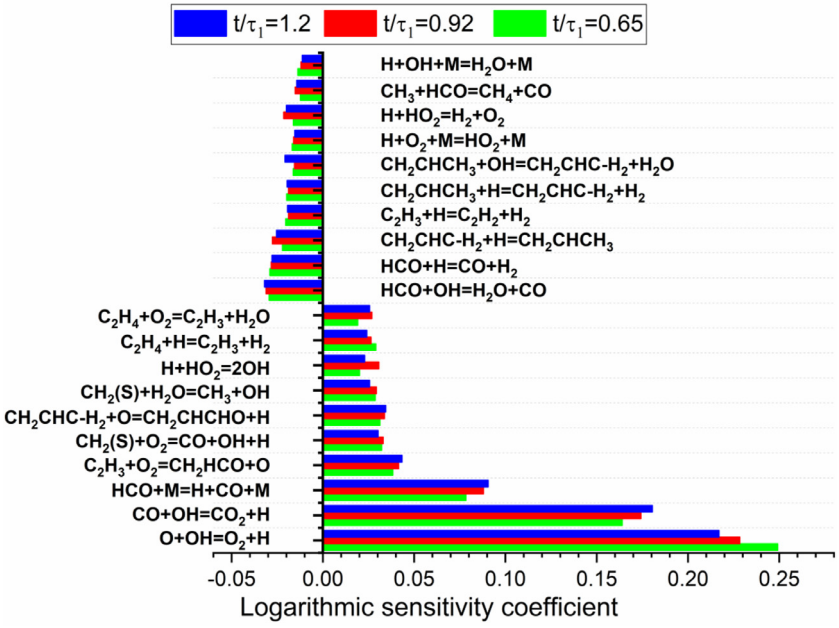

Fig. 14. Sensitivity analysis of steady premixed flames in three mixtures with different reaction progress t/τ_1= 0.65, 0.92 and 1.2 following the ignition trajectory.

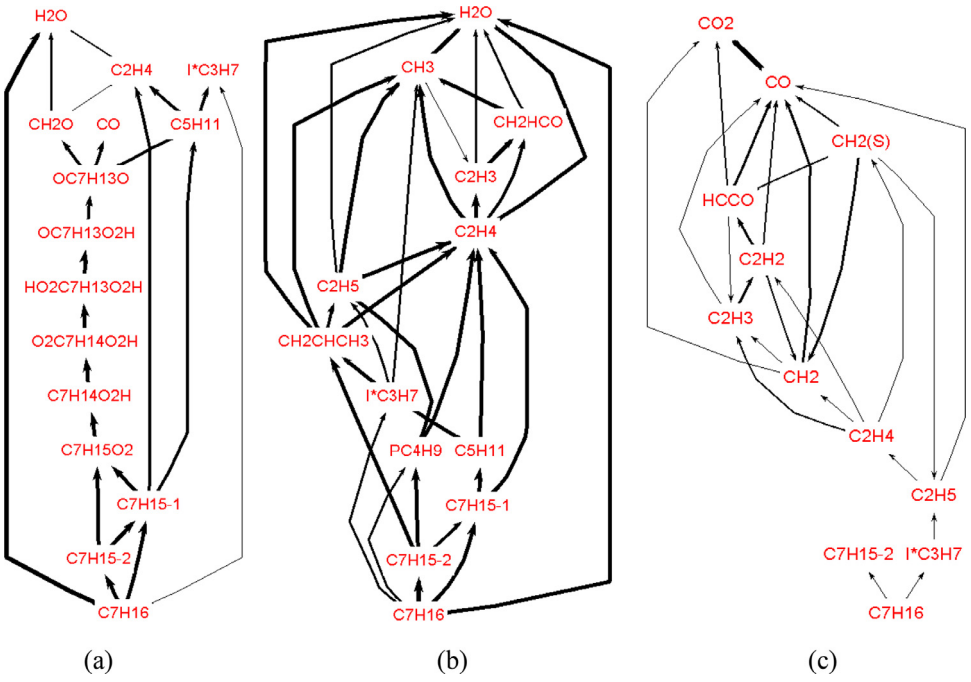

Fig. 15. Reaction network at selected (a)upstream, (b)flame front and (c) downstream locations for the flame with unburnt reaction progress $t/\tau_1 = 0.65$.

on the other hand, although the low temperature reactions are not directly associated with a large sensitivity coefficient, the low temperature products and their derivatives appear in many key reactions. For example, CH_2O is known to be a major product from low temperature chain branching reactions, which is also a primary source for the formation of HCO. It is clear that HCO participates in many key reactions that facilitate and retard flame propagation including the chain branching HCO+M = H+CO+*M*, and chain terminations HCO+H = CO+H_2, HCO+OH = H_2O+CO. This point is however not emphasized in the recent work by [24].

Chemical reaction network analysis is further conducted to understand the controlling chemical at different locations within the flame structure with unburnt reaction progress, as shown in Fig. 15. Take the t/τ_1= 0.65 case for example, at the upstream boundary of 700 K, it is seen that the low temperature oxidation RO_2, QOOH, $QOOHO_2$, and ketone decomposition reactions play the most important role in fuel consumption. At the flame front around 1400 K, it is seen that the fuel decomposition to C1-C4 fragments becomes dominant. At downstream of the flame around 2000 K, the oxidation of C1 species and formation of CO_2 are most important. These distinct reaction network demonstrates the spatial dependence of the domain reaction pathways within the flame. The results have suggested limited importance of low temperature chemistry at the upstream of the flame, but not at the flame front and the downstream. Similar observations are obtained for the other two cases t/τ_1= 0.92 and 1.2 and are added in the Supplementary Material. Such important information about the local thermochemistry is however not properly reflected through the global sensitivity analysis of flame speed. A fair and complete evaluation on the role of low temperature chemistry in flame propagation in partially reactive mixtures therefore requires both global sensitivity analysis and local reaction network constructed from thermochemical states sampled within the flame structure.

4. Conclusion

1-D laminar flame initiation and propagation in a partially reacting n-heptane/air/He mixture with two-stage ignition is computationally investigated with detailed chemistry and transport. The study focused on the flame initiation and transition regimes with variable ignition energy and reaction progress before and after the first-stage ignition under isobaric condition, where a variety of flame regimes are observed, including both hot and cool flames, as well as two types of double flames. Detailed findings and conclusions are summarized below:

(1) For flame initiation with zero reaction progress, hot flames can be triggered for relatively large ignition energies. These hot flames all collapse in speed when approaching quasi-steady. Autoignition-assisted cool flames are triggered for relatively low ignition energies. Different from the hot flame, these cool flames each take a unique path in the speed phase plot.

(2) For flame initiation in mixture with reaction progress t/τ_1 < 0.65, the coupling between ignition and flame propagation are weak and the laminar flame speed shows insensitive dependence on the unburnt mixture reaction progress. For flame initiation in mixtures with high reaction progress (t/τ_1around unity or higher), autoignition and flame propagation are strongly coupled, and the flame propagation in a post first-stage ignition mixture is substantially increased, which also has insensitive dependence on the reaction progress t/τ_1. For cases with reaction progress in between, substantial change in flame properties is observed prior to first-stage ignition and the flame speed is not well-defined. Once first-stage ignition occurs, a bump appears in the flame speed phase plot due to thermal expansion, a hot flame eventually transitions to the high reaction progress scenarios with well-defined properties regardless of any historical effects.

(3) Well-defined steady laminar flames with non-negligible upstream reaction progress can be calculated with sufficiently short upstream while sufficiently long downstream domain length, in the classical diffusion-reaction limit. The good agreement between steady and unsteady simulation suggests the quasi-steady nature of the planar flame propagation as long as $\tau_{chem}/\tau_{flame}>>1$, which is also justified by the budget term analysis. When τ_{chem} and τ_{flame} are of sim-

ilar orders of magnitude, the interaction of pressure wave and flame becomes significant, and the flame propagation becomes highly transient.

(4) Fundamental flame properties including flame speed, flame thickness and flame burning flux all increase in the post first-stage ignition mixtures, as compared to the conditions with upstream reaction progress prior-to first-stage ignition.

(5) Two kinds of double flames are observed, one is hot flame induced and the other one is cool flame induced. Given their fast transition, no obvious effects have been found on the subsequent flame propagation in the current condition.

(6) Ignition energy and ignition timing can be used as control knobs to initiate flames in different flame regimes and achieve desired flame mode transition. The choice of ignition energy and ignition timing can trigger regular hot flame, cool flame, and autoignition-assisted flames. Without quantifying the ignition energy deposition, it is possible to misinterpret the experimental observation. The relative significance of ignition energy also depends on the ignition timing, and in general, their effects are coupled and should be carefully quantified to control the flame initiation and transition.

(7) Carefully conducted sensitivity analysis with sufficiently small time ratio $\tau_{\text{flame}}/\tau_{\text{chem}}$ has been conducted, which suggests similar controlling chain branching reactions as in regular flames, such as H + O_2 = O+OH, CO+OH = CO_2+H. While no direct significance has been found in the sensitivity coefficient of the low temperature chemistry, the low temperature products and derivatives participate in some of the key reactions, including the chain branching HCO+M = H+CO+M, and chain terminations HCO+H = CO+H_2, HCO+OH = H_2O+CO. Reaction network analysis using absolute rate of production further confirms the limited importance of low temperature chemistry upstream of the flame, while fuel decomposition and CO_2 formation are dominant in the flame front and downstream, respectively. A fair and accurate evaluation on the role of low temperature chemistry therefore requires information from both the global sensitivity analysis and the local chemical network sampled within the flame.

Declaration of Competing Interest

The authors declare that they have no known competing financial interests or personal relationships that could have appeared to influence the work reported in this paper.

Acknowledgments

P.Z. is supported by the start-up grant from the University of Tennessee Space Institute. The authors acknowledge the High-Performance Computing Center (HPCC) at Texas Tech University at Lubbock for providing HPC resources that have contributed to the research results reported within this paper.

Supplementary materials

Supplementary material associated with this article can be found, in the online version, at doi:10.1016/j.combustflame.2021.111765.

References

[1] F.N. Egolfopoulos, N. Hansen, Y. Ju, K. Kohse-Höinghaus, C.K. Law, F. Qi, Advances and challenges in laminar flame experiments and implications for combustion chemistry, Prog. Energy Combust. Sci. 43 (2014) 36–67.
[2] H.H. Kim, S.H. Won, J. Santner, Z. Chen, Y. Ju, Measurements of the critical initiation radius and unsteady propagation of n-decane/air premixed flames, Proc. Combust. Inst. 34 (2013) 929–936.
[3] S. Sayama, M. Kinoshita, Y. Mandokoro, T. Fuyuto, Spark ignition and early flame development of lean mixtures under high-velocity flow conditions: an experimental study, Int. J. Engine Res. 20 (2019) 236–246.
[4] P. Zhao, W. Liang, S. Deng, C.K. Law, Initiation and propagation of laminar premixed cool flames, Fuel 166 (2016) 477–487.
[5] Combustion Webinar Series: From hotspot flame initiation to Li-ion battery thermal runaway, Nov 7, 2020, https://www.youtube.com/watch?v=gAm_pBx0JeE
[6] K.J. Bosschaart, L.P.H. de Goey, The laminar burning velocity of flames propagating in mixtures of hydrocarbons and air measured with the heat flux method, Combust. Flame 136 (2004) 261–269.
[7] S. Hu, J. Gao, C. Gong, Y. Zhou, X.S. Bai, Z.S. Li, M. Alden, Assessment of uncertainties of laminar flame speed of premixed flames as determined using a Bunsen burner at varying pressures, Appl Energy 227 (2018) 149–158.
[8] S.G. Davis, C.K. Law, Determination of and fuel structure effects on laminar flame speeds of C1 to C8 hydrocarbons, Combust. Sci. Technol. 140 (1998) 427–449.
[9] F. Wu, C.K. Law, An experimental and mechanistic study on the laminar flame speed, Markstein length and flame chemistry of the butanol isomers, Combust. Flame 160 (2013) 2744–2756.
[10] E.A. Ortiz-Soto, G.A. Lavoie, M.S. Wooldridge, D.N. Assanis, Thermodynamic efficiency assessment of gasoline spark ignition and compression ignition operating strategies using a new multi-mode combustion model for engine system simulations, Int. J. Engine Res. 20 (2019) 304–326.
[11] Z. Wang, Y. Qi, X. He, J. Wang, S. Shuai, C.K. Law, Analysis of pre-ignition to super-knock: hotspot-induced deflagration to detonation, Fuel 144 (2015) 222–227.
[12] Q. Yang, P. Zhao, Minimum ignition energy and propagation dynamics of laminar premixed cool flames, Proc. Combust. Inst. 38 (2021) 2315–2322.
[13] T. Zhang, Y. Ju, Structures and propagation speeds of autoignition-assisted premixed n-heptane/air cool and warm flames at elevated temperatures and pressures, Combust. Flame 211 (2020) 8–17.
[14] A. Krisman, E. Hawkes, J. Chen, The structure and propagation of laminar flames under autoignitive conditions, Combust. Flame 188 (2018) 399–411.
[15] Q. Yang, Z. Chen, A. Susa, R.K. Hanson, P. Zhao, Thermal-pyrolysis induced over-driven flame and its potential role in the negative-temperature dependence of iso-octane flame speed at elevated temperatures, Combust. Flame 223 (2021) 65–76.
[16] Y. Ju, Understanding cool flames and warm flames, Proc. Combust. Inst. 38 (2021) 83–119.
[17] Y. Ju, C.B. Reuter, O.R. Yehia, T.I. Farouk, S.H. Won, Dynamics of cool flames, Prog. Energy Combust. Sci. 75 (2019) 100787.
[18] A. Kazakov, Chaos M, Z. Zhao, F.L. Dryer, Computational perturbation analysis of two-stage ignition of large hydrocarbons, J. Phys. Chem. A 110 (2016) 7003–7009.
[19] C.K. Law, Combustion Physics, Cambridge University Press, 2006.
[20] J. Martz, H. Kwak, H. Im, G.A. Lavoie, Combustion regime of a reacting front propagating into an auto-igniting mixture, Proc. Combust. Inst. 33 (2011) 3001–3006.
[21] J. Martz, G.A. Lavoie, H.G. Im, R.J. Middleton, The propagation of a laminar reaction front during end gas autoignition, Combust. Flame 159 (2012) 2077–2086.
[22] J. Pan, H. Wei, G. Shu, Z. Chen, P. Zhao, The role of low temperature chemistry in combustion mode development under elevated pressures, Combust. Flame 174 (2016) 179–193.
[23] E.M. Faghih, H. Li, X. Gou, Z. Chen, On laminar premixed flame propagating into autoigniting mixtures under engine-relevant conditions, Proc. Combust. Inst. 37 (2019) 4673–4680.
[24] A. Ansari, J. Jayachandran, F. Egolfopoulos, Parameters influencing the burning rate of laminar flames propagating into a reacting mixture, Proc. Combust. Inst. 37 (2019) 1513–1520.
[25] H. Lin, P. Zhao, H. Ge, A computational study on laminar flame propagation in mixtures with non-zero reaction progress, SAE (2019) 0946 01.
[26] A.M. Feris, A.J. Susa, D.F. Davidson, R.K. Hanson, High-temperature laminar flame speed measurement in a shock tube, Combust. Flame 205 (2019) 241–252.
[27] A.J. Susa, A.M. Ferris, D.F. Davidson, R.K. Hanson, Experimental shock tube measurement of laminar burning velocity of n-heptane and iso-octane in the negative temperature coefficient regime, AIAA SciTech 2019 Forum, AIAA (2019), p. 0460.
[28] A.J. Susa, A.M. Ferris, D.F. Davidson, R.K. Hanson, Experimental observation of negative temperature dependence in iso-octane burning velocities, AIAA J. 57 (2019) 4476–4481.
[29] A. Susa, A. Ferris, D. Davidson, R. Hanson, Experimental Measurement of Laminar Burning Velocity of n-Heptane at Variable Extents of Reaction in a Shock Tube. Proceedings of the 32nd International Symposium on Shock Waves (2019) doi:10.3850/978-981-11-2730-4_0149-cd
[30] T. Zhang, A. Susa, R. Hanson, Y. Ju, Studies of the dynamics of autoignition-assisted outwardly propagating spherical cool and double flames under shock–tube conditions, Proc. Combust. Inst. 38 (2021) 2275–2283.
[31] Q. Yang, P. Zhao, H. Ge, reactingFoam-SCI: an open source CFD platform for reacting flow simulation, Computers and Fluids 190 (2019) 114–127.
[32] M. Tao, Q. Yang, P. Lynch, P. Zhao, Auto-ignition and reaction front dynamics in mixtures with temperature and concentration stratification, Front. Mech. Eng. 6 (2020) 68.

[33] H. Chen, M. Tao, Q. Yang, H. Ge, P. Zhao, Two-stage autoignition and combustion mode evolution in boundary layer flows above a cold flat plate, Proc. Combust. Inst. 38 (2021) 767–776.
[34] J.C.G. Andrae, Comprehensive chemical kinetic modeling of toluene reference fuels oxidation, Fuel 107 (2013) 740–748.
[35] J. Li, Z.W. Zhao, A. Kazakov, F.L. Dryer, An updated comprehensive kinetic model of hydrogen combustion, Int. J. Chem. Kinet. 36 (2004) 566–575.
[36] W. Zhang, M. Faqih, X. Gou, Z. Chen, Numerical study on the transient evolution of a premixed cool flame, Combust. Flame 187 (2018) 129–136.
[37] Y. Ju, On the propagation limits and speeds of premixed cool flames at elevated pressures, Combust. Flame 178 (2017) 61–69.
[38] Y. Ju, W. Sun, M.P. Burke, X. Gou, Z. Chen, Multi-timescale modeling of ignition and flame regimes of n-heptane-air mixtures near spark assisted homogeneous charge compression ignition conditions, Proc. Combust. Inst. 33 (2011) 1245–1251.
[39] J. Pan, G. Shu, P. Zhao, H. Wei, Z. Chen, Interactions of flame propagation, auto-ignition and pressure wave during knocking combustion, Combust. Flame 164 (2016) 319–328.
[40] D. Bradley, G.T. Kalghatgi, Influence of auto-ignition delay time characteristics of different fuels on pressure waves and knock in reciprocating engines, Combust. Flame 156 (2009) 2307–2318.
[41] X. Gu, D. Emerson, D. Bradley, Modes of reaction front propagation from hot spots, Combust. Flame 133 (2003) 63–74.
[42] J. Smolke, F. Carbone, F.N. Egolfopoulos, H. Wang, Effect of n-dodecane decomposition on its fundamental flame properties, Combust. Flame 190 (2019) 65–73.